Density functional study on the structures and thermodynamic properties of small ions around polyanionic DNA

Ke Wang, Yang-Xin Yu,* and Guang-Hua Gao†
Department of Chemical Engineering, Tsinghua University, Beijing, 100084, People's Republic of China
and State Key Laboratory of Chemical Engineering, Tsinghua University, Beijing 100084, People's Republic of China
(Received 20 January 2004; published 28 July 2004)

A density functional theory (DFT) is presented for describing the distributions of small ions around an isolated infinitely long polyanionic DNA molecule in the framework of the restricted primitive model. The hard-sphere contribution to the excess Helmholtz energy functional is derived from the modified fundamental measure theory, and the electrostatic interaction is evaluated through a quadratic functional Taylor expansion. The predictions from the DFT are compared with integral equation theory (IET), the nonlinear Poisson-Boltzmann (PB) equation, and computer simulation data for the ionic density profiles, electrostatic potentials, and charge compensation functions at varieties of solution conditions. Good agreement between the DFT and computer simulations is achieved. The charge inversion phenomena of DNA are observed in a moderately concentrated solution of 2:1 and 2:2 electrolytes using the DFT, IET, and computer simulation, but can never be predicted from the PB equation. The predictions of charge inversion from the DFT prove to be more accurate than those from the IET when compared with computer simulation data. The preferential interaction coefficients from the DFT are also compared with those from the PB equation and Monte Carlo simulation, and it is shown that the DFT is superior to the PB equation.

DOI: 10.1103/PhysRevE.70.011912 PACS number(s): 87.15.Nn, 82.35.Rs

I. INTRODUCTION

Deoxyribonucleic acid (DNA) is a well-known substance as a carrier of genetic information. Besides its biological function, the polyanionic DNA molecule exhibits typical polyelectrolyte features in aqueous solution. The interactions between the polyion and surrounding small ions are of significance for DNA conformational stability, as well as other thermodynamic and transport properties in solution [1–3].

The studies of physical properties of DNA solution started about 35 years ago, when the famous counterion condensation (CC) theory was established by Manning [4]. This theory is based on the experimental phenomenon of CC on the surface of a strongly charged polyion. Manning's work includes two theories: one is proposed to describe the infinitely dilute solution, and is successfully applied to calculating the limiting laws of thermodynamic properties [5,6]; the other adopts a simple two-phase model to describe solutions at moderate salt concentrations, in which the corresponding ionic profiles are derived by minimizing the free energy [7]. Recently, the CC theory was extended to take account of both finite CC and actual structure of the array of discrete charges by Schurr and Fujimoto [8] with an alternative auxiliary assumption. A further modification was also carried out to extend the CC theory to cell model and to calculate the osmotic pressure of relatively concentrated DNA solution [9].

An alternative classical theory is Poisson-Boltzmann (PB) equation, which is the Euler-Lagrange equation corresponding to the mean-field density functional of an electrolyte of point charges [10,11]. Unlike the CC theory, the PB equation is not confined to polyions of cylindrical symmetry [4]. For example, its linear version has been used to calculate the electrostatic potential around biopolymer with most complicated geometry [12]. However, it has proved that the PB equation is invalid if concentration of added salt is high [13], since the volume effect between small ions has evident effects on the total excess free energy under these conditions [14]. Large errors were also reported in the PB calculations for multivalent electrolyte even at low ionic concentrations when compared with Monte Carlo (MC) simulations [15,16].

Experiments have confirmed that multivalent cations, such as magnesium $(2+)$ and Putrescine $(2+)$, play substantial roles in many molecular biological processes involving protein-nucleic acid interactions and conformational transition of functional biopolymers [17,18]. The nonviral gene transfer in biological studies or gene therapy for clinical treatment also needs DNA condensation induced by multivalent cations or multivalent cationic amphiphiles in aqueous solution [19–22]. Furthermore, in the systems containing the multivalent counterions at high concentrations, an interesting phenomenon, termed "charge inversion" or "overcharging," was observed [20], where a strongly charged polyion binds more ions than necessary to neutralize its own charge. This phenomenon was observed in electrophoretic mobility by Strauss, Gershfeld, and Spiera [23], which is considered to be induced by volume exclusion of small ions [24,25]. However, the classical PB theory has proved unable to predict charge inversion in above conditions [26]. This deficiency of the PB theory is mainly due to its ignorance of the ionic size. Over the past 40 years, various modifications of the PB equations [15,27,28] have been developed in the framework of the restricted primitive model (RPM) of electrolyte solu-

*Corresponding author. Electronic address: yangxyu@mail.tsinghua.edu.cn
†Electronic address: gaogh@mail.tsinghua.edu.cn

tion, where the small ions are modeled as charged particles of uniform size, and the solvent is a continuous dielectric continuum. Incorporating the excluded volume effect, various versions of modified PB theories have been successfully applied to the systems involving planar electrode [29], spherical macroion [30], and linear polyelectrolyte [31,32] with multivalent ions at high salt concentrations.

An alternative way to include ionic correlations is using integral equation theory (IET) or density functional theory (DFT). Both theories involve the hard-sphere (HS) correlation due to ionic size. IET originated from the study of homogeneous electrolyte solution. The original Ornstein-Zernike equation of IET is popularly solved using hypernetted chain (HNC) closure [33]. There are two versions of HNC closure proposed for the study of polyelectrolyte solution: hypernetted chain/hypernetted chain (HNC/HNC) [34] and hypernetted chain/mean spherical approximation (HNC/MSA) [33,35]. Since the HNC/MSA theory has proved to be much more convenient and accurate than HNC/HNC [35], it has been extensively used in the calculation of ionic profiles and electrostatic potential for the system involving various geometries [33–37]. Unlike the PB and HNC, DFT starts with the simple thermodynamic principle that the system reaches equilibrium as its grand canonical potential reaches minimum [38]. Many studies of DFT have been carried out for the electrolyte solution next to the charged or uncharged surface with simple geometries, such as planar [39,40], spherical [41], and cylindrical surfaces [42,43]. It has been reported that the results from DFT agree well with MC simulation, better than those from other theories [41,42,44]. Since both of DFT and HNC/MSA take into account the excluded volume effect of small ions, both of them are adequate for observing the phenomenon of overcharging. However, recent work of Deserno *et al.* [45] has shown that HNC/MSA quantitatively overestimates overcharging if the charge density of polyion or the bulk concentration of added salt is high. In contrast, DFT predict overcharging of spherical polyion and planar electrode accurately with respect to MC results, even at high salt concentration or for intensively charged objects [39,41,46].

In the present work, a partially perturbative DFT for an isolated model DNA immersed in an electrolyte solution is proposed. In the standard DFT, the excess Helmholtz energy functional is divided into several parts due to various interactions. The hard-sphere (HS) contribution to total excess free energy is usually evaluated through a weighted-density approximation (WDA) [47]. Recently, Yu and Wu [48,49] improved Rosenfeld's fundamental measure theory [50–52] for HS correlation functions. Since this new WDA proves more accurate than other theories [48], we adopt it in our present work. Similar to the approaches employed by Yu, Wu, and Gao [41] and Patra and Yethiraj [42], the electrical interaction term is obtained using a quadratic Taylor expansion with respect to a uniform fluid. The established DFT is used to calculate the microscopic properties of mobile ions, i.e., ionic density profiles, electrostatic potential profiles, and charge compensation functions, as well as thermodynamic property of preferential interaction coefficients. These results are compared with those from the PB equation, IET, and molecular simulations [45,53–55].

The rest of this paper is organized as follows. Section II describes the DFT theory for interested systems. Numerical solutions for the ionic density profiles, mean electrostatic potentials, charge compensation functions, and preferential interaction coefficients are presented in Sec. III. The conclusions and perspectives for future work are given in Sec. IV.

II. THEORY

A. Molecular model

We consider an isolated double-stranded DNA molecule in an electrolyte solution. The polyion of DNA is modeled as an infinitely long, impenetrable cylinder with uniformly distributed charges along its central axis. Since there are various conformations of DNA molecules in aqueous solution, we propose a model B-DNA, in which the average charge spacing on the DNA molecule is $b=0.17$ nm and the radius of DNA is $R=0.80$ nm. All species of ions are modeled as charged hard spheres with equal diameters $d_\alpha=0.40$ nm, and the minimal separation between ions and axis of the polyion is 1.0 nm. Both the radius and diameter given above have taken into account the effect of hydration. The solvent water is modeled as a continuous structureless media with invariant dielectric constant $\varepsilon=78.4$ at any position, corresponding to that of the pure water at $T=298$ K. The temperature of system is $T=298$ K. All the parameters given above are applied in the main part of this work, but to compare with the molecular simulation data they may be changed in consistence with the corresponding literature and are pointed out in the captions.

B. Density functional theory

In grand canonical ensemble, the system reaches equilibrium when the grand canonical potential Ω is at its minimum value $\tilde{\Omega}$. By virtue of variational principle, the equilibrium distribution of ion i, $\{\tilde{\rho}_i\}$, is obtained from Euler equation

$$\left.\frac{\delta\Omega[\{\rho_i\}]}{\delta\rho_i(r)}\right|_{\tilde{\rho}}=0, \quad \Omega[\{\rho_i\}]|_{\tilde{\rho}}=\tilde{\Omega}. \tag{1}$$

For the system studied in this work, the grand potential for small ions surrounding a DNA molecule can be expressed as a functional of Helmholtz energy for density profile of certain species $\{\rho_i\}$ through the Legendre transform

$$\Omega[\{\rho_i\}]=F[\{\rho_i\}]+\sum_{i=1}^{N}\int d\mathbf{r}[V_{Pi}(\mathbf{r})-\mu_i]\rho_i(\mathbf{r}) \tag{2}$$

where $V_{Pi}(\mathbf{r})$ is external field due to the DNA molecule, N is the total number of ionic species, μ_i is the chemical potential of ion i, and $F[\{\rho_i\}]$ represents the Helmholtz energy functional.

Then the problem focuses on finding out an accurate and explicit expression of Helmholtz energy functional. In general, Helmholtz energy functional can be divided into two terms

$$F[\{\rho_i\}]=F^{\mathrm{id}}[\{\rho_i\}]+F^{ex}[\{\rho_i\}] \tag{3}$$

where the first term on right of Eq. (3) is the ideal-gas contribution, the second term is the excess Helmholtz energy

due to the interactions between ions. $F^{\mathrm{id}}[\{\rho_i\}]$ is obtained accurately from classical statistical mechanics

$$F^{\mathrm{id}}[\{\rho_i\}] = k_B T \sum_{i=1}^{N} \int dr \rho_i(\mathbf{r})\{\ln[\rho_i(\mathbf{r})\Lambda_i^3] - 1\} \tag{4}$$

where Λ_i is the thermal wavelength of component i and k_B is the Boltzmann constant. $F^{\mathrm{ex}}[\{\rho_i\}]$ can be further decomposed into several parts according to different types of interactions. In the present work, $F^{\mathrm{ex}}[\{\rho_i\}]$ is divided into three parts, i.e.,

$$F^{\mathrm{ex}}[\{\rho_i\}] = F_{\mathrm{C}}^{\mathrm{ex}}[\{\rho_i\}] + F_{\mathrm{hs}}^{\mathrm{ex}}[\{\rho_i\}] + F_{\mathrm{el}}^{\mathrm{ex}}[\{\rho_i\}]. \tag{5}$$

The first term is direct Coulomb contribution calculated by summing the electrostatic potential over the space

$$F_{\mathrm{C}}^{\mathrm{ex}}[\{\rho_i\}] = \frac{1}{2}\int\int d\mathbf{r} d\mathbf{r}' \sum_{i,j} \frac{z_i z_j e^2 \rho_i(\mathbf{r})\rho_j(\mathbf{r}')}{\varepsilon|\mathbf{r}-\mathbf{r}'|}. \tag{6}$$

The second and the third terms in Eq. (5) denote HS contribution and coupling of Coulombic and HS interactions, respectively. According to the modified fundamental measure theory (MFMT) [48], $F_{\mathrm{hs}}^{\mathrm{ex}}[\{\rho_i\}]$ takes the form

$$F_{\mathrm{hs}}^{\mathrm{ex}} = k_B T \int \Phi^{\mathrm{hs}}[n_\alpha(\mathbf{r})] d\mathbf{r} \tag{7}$$

where $\Phi^{\mathrm{hs}}[n_\alpha(\mathbf{r})]$ is the reduced excess Helmholtz energy density due to HS correlation, and $n_\alpha(\mathbf{r})$ is the weighted density, given by

$$n_\alpha(\mathbf{r}) = \sum_{i=1}^{N} n_{\alpha i}(\mathbf{r}) = \sum_{i=1}^{N} \int \rho_i(\mathbf{r}') w_i^{(\alpha)}(\mathbf{r}'-\mathbf{r}) d\mathbf{r}' \tag{8}$$

where the subscripts $\alpha = 0$, 1, 2, 3, V1, and V2 denote the indices of six weight functions $w_i^{(\alpha)}(\mathbf{r})$, i.e.,

$$w_i^{(0)}(r) = \frac{\delta(\sigma_i/2 - r)}{\pi\sigma_i^2}, \tag{9}$$

$$w_i^{(1)}(r) = \frac{\delta(\sigma_i/2 - r)}{2\pi\sigma_i}, \tag{10}$$

$$w_i^{(2)}(r) = \delta(\sigma_i/2 - r), \tag{11}$$

$$w_i^{(3)}(r) = \theta(\sigma_i/2 - r), \tag{12}$$

$$\mathbf{w}_i^{(V2)}(\mathbf{r}) = (\mathbf{r}/r)\delta(\sigma_i/2 - r), \tag{13}$$

$$\mathbf{w}_i^{(V1)}(\mathbf{r}) = \frac{(\mathbf{r}/r)\delta(\sigma_i/2 - r)}{2\pi\sigma_i} \tag{14}$$

where $\delta(r)$ is the Dirac delta function and $\theta(r)$ denotes the Heaviside step function. $w_i^{(2)}(r)$, $w_i^{(3)}(r)$, and $\mathbf{w}_i^{(V2)}(\mathbf{r})$ are directly related to the geometry of a spherical particle.

According to the MFMT [48], the HS Helmholtz energy density is divided into the scalar weighted densities (S) and the vector weighted densities (V)

$$\Phi^{\mathrm{hs}}[n_\alpha(\mathbf{r})] = \Phi^{\mathrm{hs(S)}}[n_\alpha(\mathbf{r})] + \Phi^{\mathrm{hs(V)}}[n_\alpha(\mathbf{r})]. \tag{15}$$

Both of the terms on the right of Eq. (15) are evaluated as functions of weighted density $n_\alpha(\mathbf{r})$

$$\Phi^{\mathrm{hs(S)}}[n_\alpha(\mathbf{r})] = -n_0 \ln(1-n_3) + \frac{n_1 n_2}{1-n_3} + \frac{n_2^3 \ln(1-n_3)}{36\pi n_3^2} + \frac{n_2^3}{36\pi n_3 (1-n_3)^2} \tag{16}$$

and

$$\Phi^{\mathrm{hs(V)}}[n_\alpha(\mathbf{r})] = -\frac{\mathbf{n}_{V1}\cdot\mathbf{n}_{V2}}{1-n_3} - \frac{n_2 \mathbf{n}_{V2}\cdot\mathbf{n}_{V2}}{12\pi n_3^2}\ln(1-n_3) - \frac{n_2 \mathbf{n}_{V2}\cdot\mathbf{n}_{V2}}{12\pi n_3 (1-n_3)^2}. \tag{17}$$

$F_{\mathrm{el}}^{\mathrm{ex}}[\{\rho_i\}]$ is obtained through a second-order functional Taylor expansion of the residual Helmholtz free energy around a uniform fluid [41]:

$$\beta F_{\mathrm{el}}^{\mathrm{ex}}[\{\rho_i\}] = \beta F_{\mathrm{el}}^{\mathrm{ex}}[\{\rho_i^b\}] - \sum_{i=1}^{N} \Delta C_i^{(1)\mathrm{el}}(\rho_i(r) - \rho_i^b) - \frac{1}{2}\sum_{i=1}^{N}\sum_{j=1}^{N} \Delta C_{ij}^{(2)\mathrm{el}}(|\mathbf{r}_i - \mathbf{r}_j|)(\rho_i(r) - \rho_i^b)(\rho_j(r) - \rho_j^b) \tag{18}$$

where $\{\rho_i^b\}$ is the bulk density of i, $\Delta C_i^{(1)\mathrm{el}}$, and $C_{ij}^{(2)\mathrm{el}}$ are direct correlation functions due to the residual electrostatic. The $\Delta C_i^{(1)\mathrm{el}}$ will finally disappear in Euler equation and $\Delta C_{ij}^{(2)\mathrm{el}}(r)$ can be evaluated explicitly by the (MSA) [56,57] from

$$\Delta C_{ij}^{(2)\mathrm{el}}(r) = \begin{cases} -\dfrac{z_i z_j e^2 \beta}{\varepsilon}\left[\dfrac{2B}{\sigma} - \left(\dfrac{B}{\sigma}\right)^2 r - \dfrac{1}{r}\right] & r < \sigma \\ 0 & r > \sigma \end{cases} \tag{19}$$

where B is given by

$$B = \frac{\kappa + 1 - (1+2\kappa)^{\frac{1}{2}}}{\kappa} \tag{20}$$

and $1/\kappa$ is known as Debye screening length calculated from

$$\kappa = \left(\frac{4\pi\beta e^2}{\varepsilon}\sum_{i=1}^{N} \rho_i^b z_i^2\right)^{1/2}. \tag{21}$$

Incorporating the explicit expressions of Helmholtz energy mentioned above, the Euler equations Eq. (1) becomes

$$\rho_i(\mathbf{r}) = \rho_i^b \exp\left\{\frac{1}{k_B T}\left[-\frac{\delta F_{\mathrm{hs}}^{\mathrm{ex}}}{\delta\rho_i(\mathbf{r})} + \mu_{i,\mathrm{hs}}^{\mathrm{ex}}\right] - \frac{z_i e}{k_B T}[\psi(\mathbf{r}) - \psi^b] + \sum_{j=1}^{N}\int d\mathbf{r}' \Delta C_{ij}^{(2)\mathrm{el}}(|\mathbf{r}'-\mathbf{r}|)[\rho_j(\mathbf{r}') - \rho_j^b]\right\} \tag{22}$$

where $F_{\mathrm{hs}}^{\mathrm{ex}}$ is evaluated from Eq. (7), $\mu_{i,\mathrm{hs}}^{\mathrm{ex}}$ is excess chemical

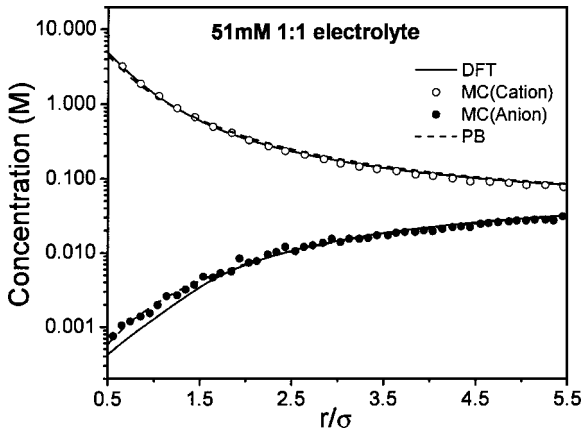

FIG. 1. Concentration profiles of a 1:1 model electrolyte around rodlike DNA molecule at bulk the concentration of 51 mM. The distance r is measured with respect to the surface of cylindrical DNA in units of the ionic diameter.

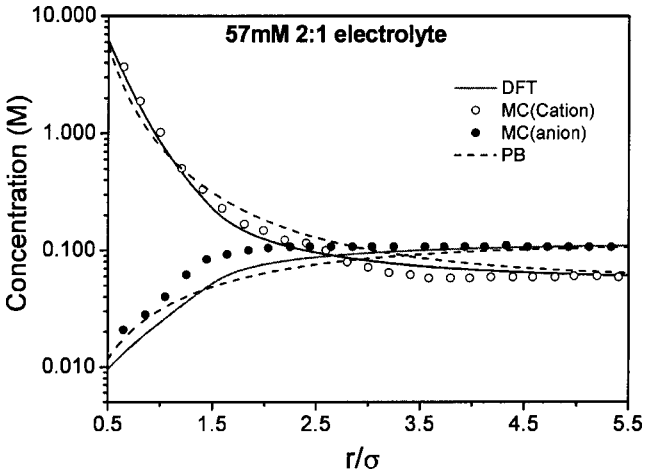

FIG. 2. Concentration profiles of a 2:1 model electrolyte around DNA molecule at the bulk concentration of 57 mM. The distance r is measured with respect to the surface of DNA in units of the ionic diameter.

potential due to HS correlation, $\psi(\mathbf{r})$ is the mean electrostatic potential obtained from solution of Poisson equation in cylindrical geometry. $\psi(\mathbf{r})$ is given by

$$\psi(r) = -\frac{4\pi e}{\varepsilon}\int_{r}^{\infty} \ln\left(\frac{r'}{r}\right)\sum_i \rho_i(r')z_i r' dr' \tag{23}$$

with the constraint of electroneutrality

$$2\pi b\int_{R}^{\infty} dr r\sum_i \rho_i(r)z_i = 1 \tag{24}$$

where r and r' are the distances between the ion center and polyion axis, the subscript i denotes the different species of ions, b is the charge spacing of DNA, and e denotes the elementary charge. If the volume exclusion of ions is ignored, $F_{\mathrm{el}}^{\mathrm{ex}}$ and $F_{\mathrm{hs}}^{\mathrm{ex}}$ become zeros, then Eq. (22) becomes

$$\rho_i(r)/\rho_i^b = \exp\left[-\beta z_i e\psi(r)\right]. \tag{25}$$

Equation (25) is the integral version of the nonlinear PB equation for cylindrical geometry.

III. RESULTS AND DISCUSSION

A. Density profile

We first compare the concentration profiles obtained from the DFT with those from MC simulation [55] and the nonlinear PB equation in Fig. 1 for 1:1 electrolyte solution at the bulk concentration of 51 mM. The curves in this figure show that ionic profiles from both the DFT and nonlinear PB equation agree well with those from MC simulation except the deviation of co-ion profile produced by the DFT in the region near DNA molecule. The similar curves are plotted for 57 mM 2:1 salt in Fig. 2. The prediction of counterion profile from the DFT is obviously better than that from the PB when compared with the MC results [55]. From Fig. 2 one can see that both the DFT and nonlinear PB are unable to describe the anionic profile accurately. However, it is noted that the deviations of anionic profiles have little effect on electrostatic potential and charge compensation function, since the local concentration of anion in vicinity of DNA is very low.

Figures 3 and 4 give ionic density profiles for 1:1 model electrolyte at bulk concentration of 0.495 M and for 2:2 model electrolyte at bulk concentration of 0.501 M, respectively. The reduced local density is defined as the ratio of local number density to bulk density or ratio of local concentration to bulk concentration, i.e., $g_i(r)=\rho_i(r)/\rho_i^b=C_i(r)/C_i^b$. From Figs. 3 and 4 one can see that the PB equation substantially underestimates the counterion accumulation in vicinity of DNA, while the ionic density profiles from DFT are

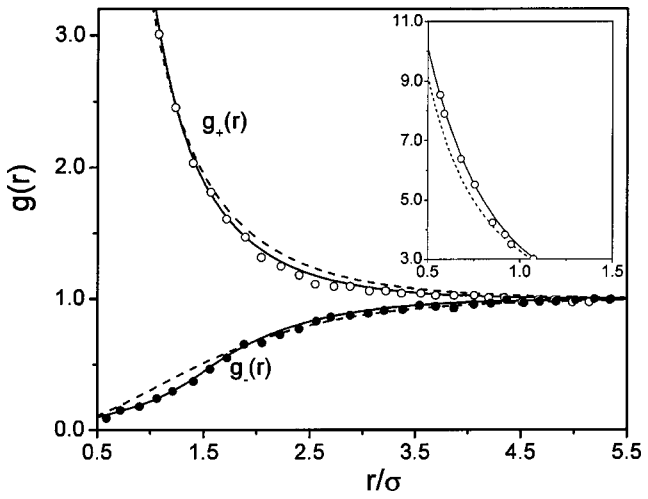

FIG. 3. Reduced density profiles for a 1:1 model electrolyte around DNA molecule at bulk concentration of 0.495M (T=298 K, R=0.9.8 nm, σ_i=0.425 nm, ε=78.5). The distance r is measured with respect to the surface of DNA in units of the ionic diameter. Circles represent MC simulation results [53]. The solid and dashed curves are predictions from the present DFT and nonlinear PB equations, respectively. The inset shows counterion profiles near contact.

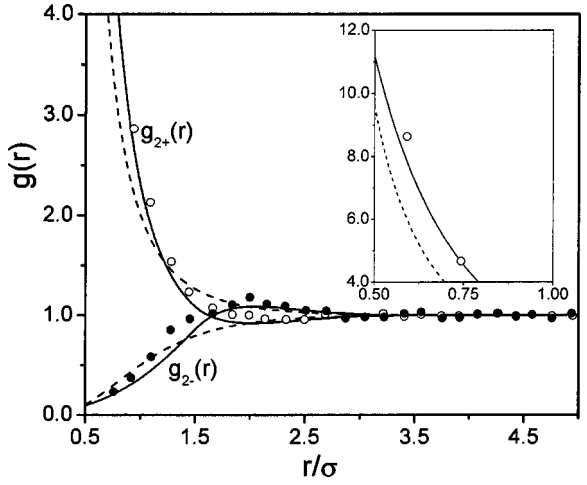

FIG. 4. Reduced density profiles for a 2:2 model electrolyte around DNA molecule at bulk concentration of 0.501M (T=298 K, R=0.98 nm, σ_i=0.425 nm, ε=78.5). The distance r is measured with respect to the surface of DNA in units of the ionic diameter. Legend is the same as Fig. 3. The inset shows counterion profiles near contact.

in good agreement with those from MC simulations [53]. This difference is caused by the ionic correlation, which is included in the MC and DFT, but neglected in the PB equation. Figure 5 compares the DFT, HNC [45], PB, and molecular dynamics (MD) [45] results for 0.49 M 2:2 electrolyte solution. The ionic profiles predicted by the HNC and DFT are almost superposed, and both of them coincide better with the MD data than the PB equation does. As shown in Figs. 4 and 5, all the MC, MD, HNC, and DFT predict a crossover of the reduced density profile $g_{2+}(r)$ and $g_{2-}(r)$ at the position about $r \approx 1.7\sigma$, while the nonlinear PB equation fails to describe this phenomenon. Crossover of $g_{2+}(r)$ and $g_{2-}(r)$ is an important symbol of overcharging, and we will return to this point later.

The ionic profiles from DFT are plotted in Fig. 6 using semilogarithmic scale for three types of salt at 1.0 M bulk

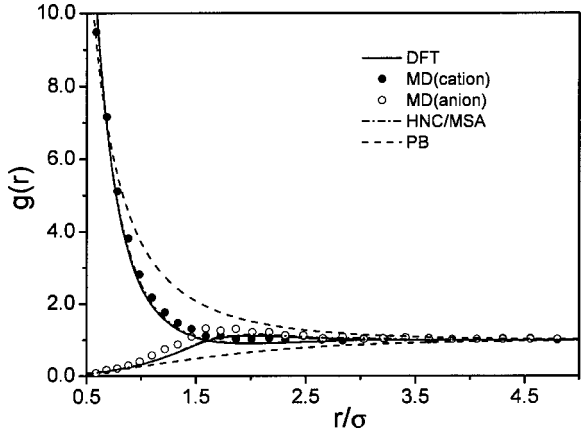

FIG. 5. Reduced density profiles for a 2:2 model electrolyte around DNA molecule at bulk concentration of 0.490 M (T =298 K, R=0.786 nm, σ_i=0.425 nm, ε=78.5). The distance r is measured with respect to the surface of DNA in units of the ionic diameter.

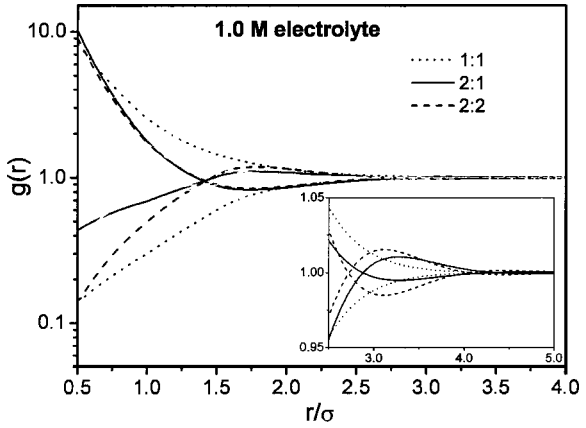

FIG. 6. Reduced density profiles from DFT for 1:1, 2:1, and 2:2 model electrolytes around DNA molecule at bulk concentration of 1.0 M. The distance r is measured with respect to the surface of DNA in units of the ionic diameter. The inset shows an enlargement of the region in which overcrosses of counterion profile and co-ion profile occur again.

concentration. Only the curves for divalent salt show crossovers of counterion and co-ion profiles.

B. Mean electrostatic potential

Mean electrostatic potential expressed as Eq. (23) is calculated from ionic profiles obtained in the above section. Figure 7 shows the electrostatic potential profiles produced by the DFT, PB, and MC simulation [53]. The curve calculated from the DFT agrees very well with the MC results, especially within r=3.0 σ. The difference between the DFT and MC results beyond $r=3.0\sigma$ is mainly due to the numerical error, which will be discussed later. The zeta potential, defined as the electrostatic potential at the distance of closest approach between ions and polyion, is $1.81 \pm 0.05 k_B T/e$ given by MC [53] and 1.87 $k_B T/e$ calculated by the DFT in this work. The difference between these two methods is un-

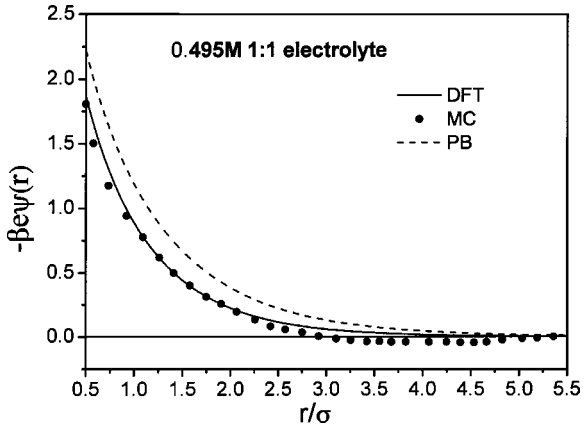

FIG. 7. Reduced mean electrostatic potential around DNA for a 1:1 electrolyte as a function of distance at the bulk concentration of 0.495 M (T=298 K, R=0.98 nm, σ_i=0.425 nm, ε=78.5). The distance r is measured with respect to the surface of DNA in units of the ionic diameter.

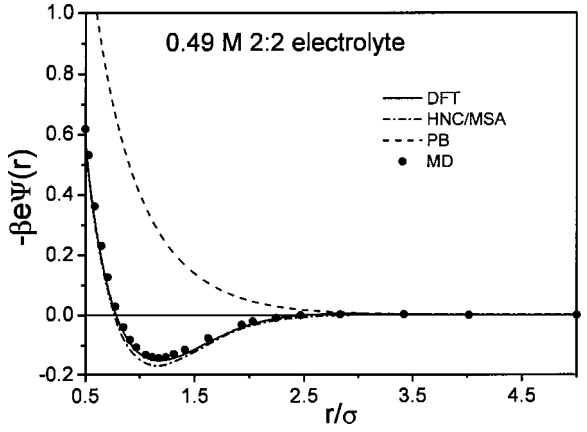

FIG. 8. Reduced mean electrostatic potential around DNA for a 2:2 electrolyte as a function of distance at the bulk concentration of 0.49 M ($T=298$ K, $R=0.786$ nm, $\sigma_i=0.425$ nm, $\varepsilon=78.5$). The distance r is measured with respect to the surface of DNA in units of the ionic diameter.

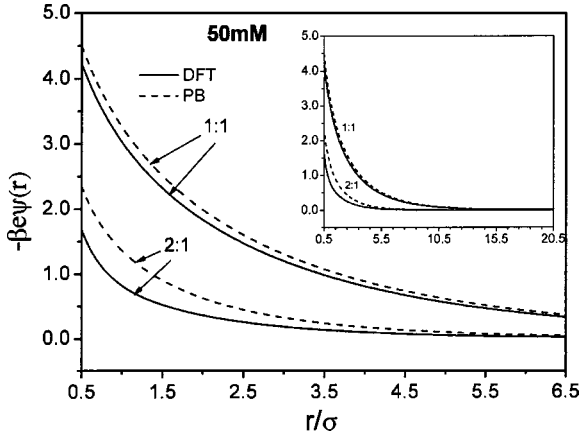

FIG. 9. Mean electrostatic potential around DNA for 2:1 and 1:1 electrolytes as a function of distance at the bulk concentration of 50 mM. The distance r is measured with respect to the surface of DNA in units of the ionic diameter. The inset gives the full curves of mean electrostatic potential over a wide range of distance.

noticeable. The mean electrostatic potential predicted by the nonlinear PB is more negative than MC results near DNA (the zeta potential predicted from the PB is 2.22 k_BT/e). As mentioned in above section, ionic correlation leads to more counterions accumulated around DNA, therefore, if volume exclusion of small ions is included the electrostatic field produced by polyion declines faster along r direction than that predicted without this consideration.

Differences among mean electrostatic potential profiles predicted by the HNC [45], DFT, PB, and MD [45] are compared in Fig. 8 for 2:2 electrolyte at the bulk concentration of 490 mM. For 1:1 electrolyte, HS contribution only accelerates counterion screen, but if counterions double their charges (such as divalent cation), electrostatic potential will reduce sharply, and even becomes positive. In Fig. 8, the electrostatic potential curve, produced by MD, goes down through the zero line at about $r\approx 0.3\sigma$ from DNA surface, and then maintains positive before it reduces to zero. Since only a positively charged object produces a positive electrostatic field around it, DNA and ions within the distance $r\approx 0.3\sigma$ just act integrally as a positively charged object. This is the characteristic of charge inversion or overcharging. This phenomenon can never be predicted by the PB equation [26], but can be predicted correctly by HNC, DFT, and computer simulation. The negative electrostatic field produced by a polyion causes an accumulated layer of counterions in the closest annular around DNA, while the positive electrostatic potential presenting beyond this layer causes another accumulated layer of co-ion. These two accumulated layers correspond to the cusps of counterion and co-ion profiles at about $r=0$ and $r\approx 2.0\sigma$, respectively, in Figs. 4 and 5. We also find that the electrostatic potentials computed from the DFT coincide very well with the MD results and are better than those predicted from the HNC. The superiority of the DFT over the HNC will be discussed theoretically in the next section.

As in Fig. 9, no charge inversion is predicted from either the PB equation or DFT in dilute solution, and the mean electrostatic potentials from the PB equation and DFT are close for 1:1 electrolyte. However, a great difference between the electrostatic potentials from the PB and DFT exists for 2:1 electrolyte even at very low concentrations.

Figure 10 gives the electrostatic potentials from the DFT for 1:1, 2:1, and 2:2 salts at the bulk concentration of 500 mM. Curves for 2:1 and 2:2 behave alike in electrostatic potential, and due to that, the extremely low concentrations of co-ion around the DNA have little effect on electrostatic potential. The electrostatic potentials for 2:1 and 2:2 electrolytes are much lower than for 1:1 electrolyte. This is because divalent cation screens the external electrostatic potential much more efficiently than monovalent cation does.

The influence of bulk concentration on the electrostatic potential for 2:1 electrolyte is predicted from the DFT and the results are shown in Fig. 11. From this figure one can see that zeta-potential decreases as bulk concentration increases. At high concentration (e.g., 1.0 M), there is a second charge inversion that occurs at the second cross of electrostatic potential curve and zero line.

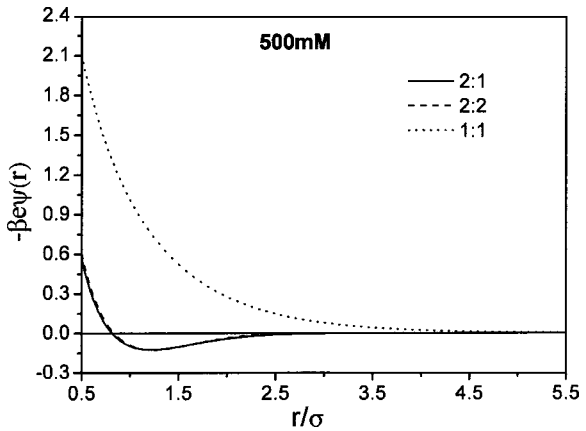

FIG. 10. Mean electrostatic potential around DNA predicted by DFT at the bulk concentration of 500 mM. The distance r is measured with respect to the surface of DNA in units of the ionic diameter.

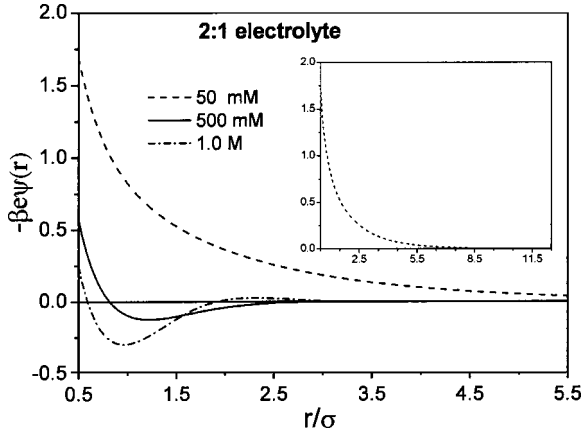

FIG. 11. Mean electrostatic potential predicted by DFT for a 2:1 electrolytes at the various bulk concentrations. The distance r is measured with respect to the surface of DNA in units of the ionic diameter. The inset shows the full curves of 0.05 M over a wide range of distance.

C. Charge compensation

To describe the process that mobile ions gradually neutralize the fixed charges on DNA surface, a charge compensation function is defined as [54]

$$Q(r) = 2\pi b \int_0^r \sum_i z_i \rho_i(r') r' dr' \tag{26}$$

where r and r' are the distance from DNA axis. $Q(r)$ represents the integral of the total charges over all species of mobile ions within the annular volume extending radially from central axis to r and axially over a length b. Since every b length on DNA surface bears one unit (elementary charge), $Q(r)$ will finally converge to unity at bulk limit obeying the electroneutrality condition.

The charge compensation curves obtained from the nonlinear PB and DFT at bulk concentration of 911 mM are compared with the MC simulation results [54] in Fig. 12. We also compare the DFT, HNC, [45], and PB with MD [45] results for 2:2 electrolyte in Figs. 13 and 14. From Figs. 12–14, one can see that charge compensation functions predicted from the PB vary monotonously along r direction and are qualitatively different from the molecular simulation results. However, the charge compensation functions for 2:2 electrolyte predicted by DFT, HNC, and MD overshoot the unity and reach their maximum. As shown in Fig. 14, at low bulk concentration, the DFT and HNC predict almost identical curves, but both of them deviate from MD results. At high bulk concentration, the HNC overestimates the charge inversion and predicts a higher peak of charge compensation function than MD does. A similar overestimation of overcharging has also been shown in the electrostatic potentials predicted by HNC in Sec. III B. However, the DFT computes the charge compensation functions correctly with respect to

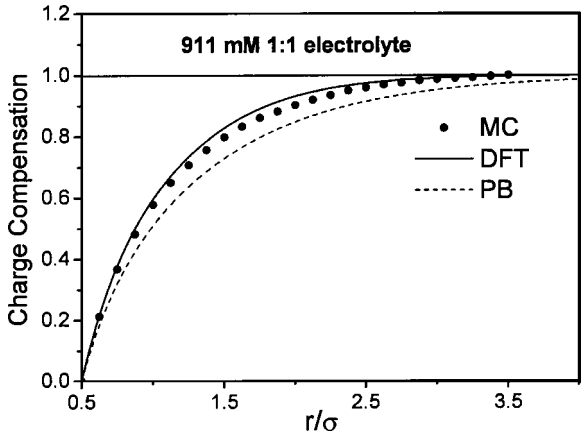

FIG. 12. Charge compensation function for a 1:1 electrolyte at 911 mM bulk concentration (T=298 K, R=0.80 nm, σ_i=0.40 nm, ε=78.358). The distance r is measured with respect to the surface of DNA in units of the ionic diameter.

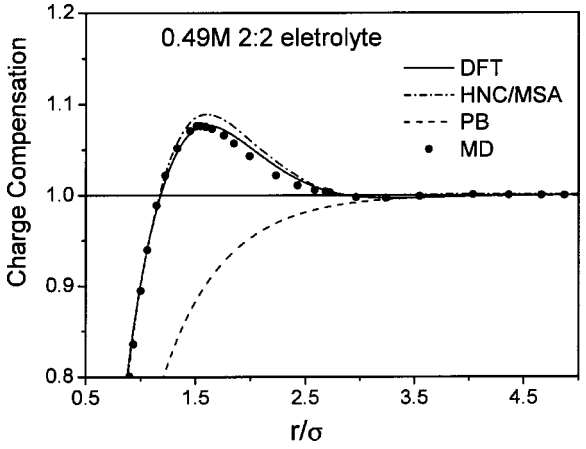

FIG. 13. Charge compensation function for a 2:2 electrolyte at 0.49 M bulk concentration (T=298 K, R=0.786 nm, σ_i=0.425 nm, ε=78.5). The distance r is measured with respect to the surface of DNA in units of the ionic diameter.

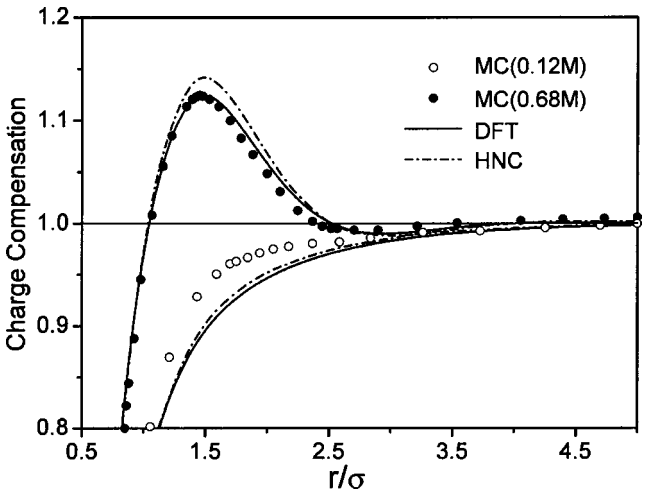

FIG. 14. Charge compensation function for a 2:2 electrolytes (T=298 K, R=0.786 nm, σ_i=0.425 nm, ε=78.5). The distance r is measured with respect to the surface of DNA in units of the ionic diameter. The curves crossing unity line correspond to the bulk concentration of 0.68 M and the others correspond to the bulk concentration of 0.12 M.

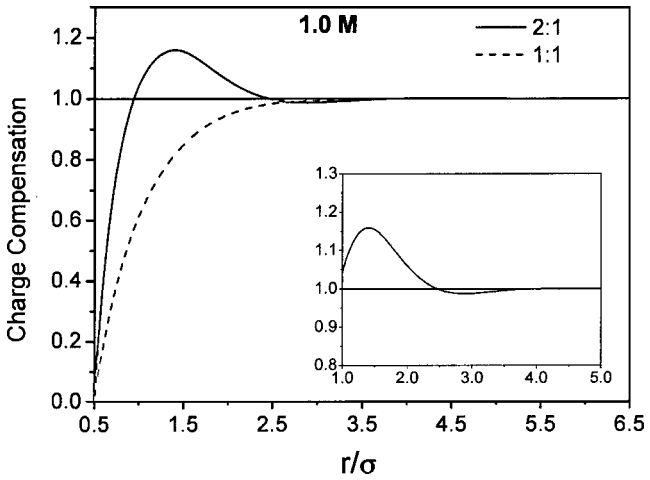

FIG. 15. Charge compensation function predicted by DFT for 1:1 and 2:1 electrolytes at 1.0 M bulk concentration. The distance r is measured with respect to the surface of DNA in units of the ionic diameter. The inset shows an enlargement of the region in which charge compensation function of 2:1 electrolyte falls down below 1.0 again.

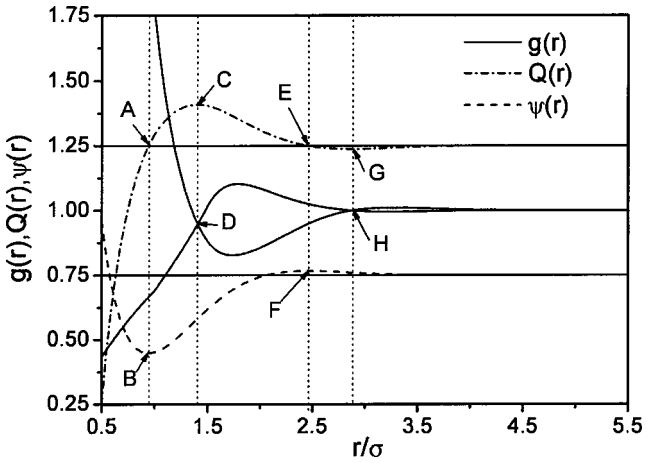

FIG. 16. Density profile, electrostatic potential, and charge compensation function from DFT for a 2:1 electrolyte at the bulk concentration of 1.0 M. The distance r is measured with respect to the surface of DNA in units of the ionic diameter. The curves for electrostatic potential and charge compensation function have upward displacements of 0.75 and 0.25, respectively.

MD results, even at the region around the peak. All above, comparisons show that the DFT is better than the HNC.

As pointed out by Deserno *et al.* [45], the overestimations of HNC/MSA with respect to MD data are probably due to two facts: (i) the excluded volume used in HNC/MSA and MD is not identical; (ii) HNC/MSA theory does not take into account all the size and charge correlations. The deviation of HNC/MSA herein are considered to be mainly due to the first reason, because the overestimation of HNC/MSA is also observed under the similar conditions in the study of Lozada-Cassou, Saavedra-Barrera, and Henderson [33]. In their study, the electrostatic potentials around charged electrode are investigated by HNC/MSA and MC simulation. Although both of the methods take the identical model of ion as charged hard spheres, the HNC/MSA somewhat overestimate the overcharging. On the other hand, excess Helmholtz functional approximation in DFT are almost identical to that in HNC/MSA, except the HS correlation, which is derived from the Carnahan-Starling equation in the DFT, and is the same as the Percus-Yevick approximation in HNC/MSA. It has proved that the Percus-Yevick approximation is not as the good as the Carnahan-Starling equation, especially in dense fluid. The HS correlation is crucial for ionic profiles around DNA, for the ions are much more crowded there. Therefore, it is believed that the improvement of the approximation of HS correlation makes DFT a better prediction of overcharging than HNC/MSA.

Interestingly, in Fig. 15 DFT predicts a minimum of charge compensation function after the maximum for 2:1 electrolyte at the bulk concentration of 1.0 M. To explain why this charge compensation function crosses the unity line twice and why the corresponding electrostatic potential crosses the zero line twice, we discuss the relationships between the ionic profile, electrostatic potential, and charge compensation function in detail. From the knowledge of electromagnetics, the electric field intensity E can be expressed as the inverse of first derivative of the electrostatic potential. We get it from Eq. (23) using electroneutrality condition

$$E(r) = -\nabla\psi(r) = \frac{4\pi e}{\varepsilon}\left(\frac{-1}{2\pi br} + \frac{1}{r}\int_0^r \sum_i z_i\rho_i(r')r'dr'\right)$$

$$= \frac{2e}{\varepsilon br}[-1 + Q(r)]. \tag{27}$$

At the position where $Q(r)$ crosses unity line, $E(r)$ changes its sign and $\psi(r)$ reaches its extremum, which is shown at the vertical auxiliary line AB or EF in Fig. 16. Then we also differentiate $Q(r)$

$$\nabla Q = 2\pi b\sum_i z_i\rho_i(r)r. \tag{28}$$

Similarly, it is easy to find out that the $Q(r)$ reaches its extremum at the place where density profiles of counterion and co-ion cross each other as shown at the vertical auxiliary line CD or GH in Fig. 16. It is concluded that when one of the three phenomena, overshoot of $Q(r)$, change of the sign of $\psi(r)$ or ionic profile overcross is found, the other two must occur simultaneously and vice versa. All of the three phenomena have the same meaning of charge inversion. Therefore, there must be something inaccurate for the points below zero in electrostatic potential curve predicted by MC in Fig. 7, because no crossover is shown in the corresponding ionic density profiles.

D. Preferential interaction coefficient

The preferential interaction coefficient characterizes the interaction between a polyion and its surrounding small ions [43,55]. For each ion species it is obtained by integrating the difference between its local density and its bulk density over the volume outside the polyions. For a cylindrical polyion

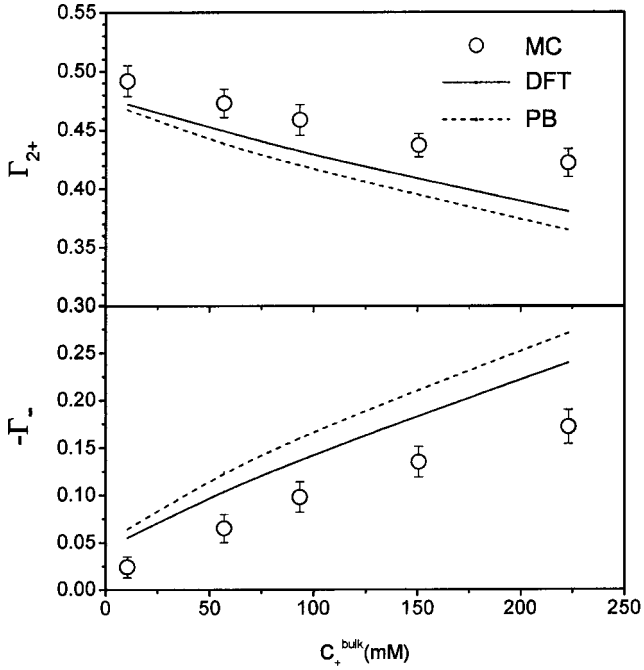

FIG. 17. DNA-ion preferential interaction coefficients for a 2:1 salt at various bulk concentrations.

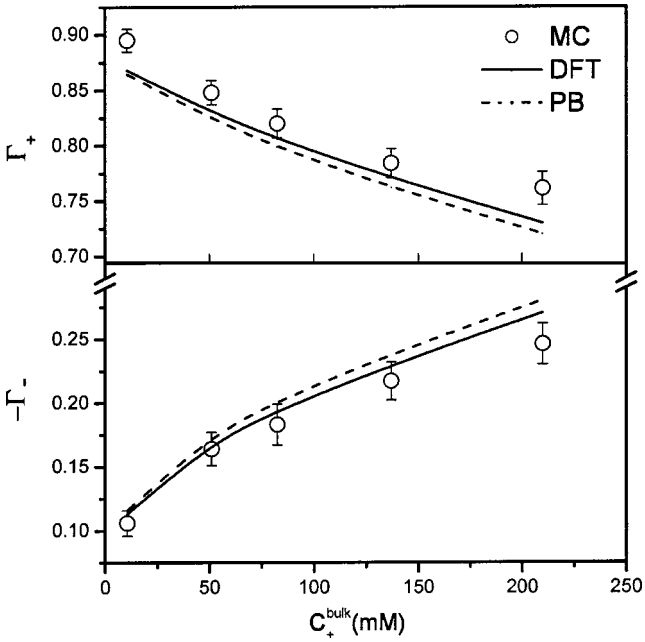

FIG. 18. DNA-ion preferential interaction coefficients for a 1:1 salt at various bulk concentrations.

one measures it with respect to the length per unit charge, leading to the definition

$$\Gamma_i = 2\pi b \int_0^\infty dr r[\rho_i(r) - \rho_i^b]. \tag{29}$$

In practice, we use a large cutoff radius R_C as the upper limit of the integral rather than infinity. R_C is selected large enough that polyions have negligible effects on small ions at $r=R_C$. If the finite concentration of polyion is considered, finite cell boundary condition is always employed in simulations and theoretical calculations [55]. Therefore, R_C must be designated less than the cell radius. In fact, the polyion concentration should be selected sufficiently dilute so that the effect of polyion dispears at cell boundary, otherwise the preferential interaction coefficient defined in Eq. (29) cannot be calculated properly. However, in the present work, each system contains only one isolated DNA molecule, therefore, any large cutoff radius is adequate. $R_C=40\sigma$ is designated for the solution with its bulk concentration not more than 100 mM, while $R_C=30\sigma$ is applied to more concentrated solution. The preferential interaction coefficients of counterion and co-ion, calculated from the DFT, MC [55], and PB for pure 2:1 and 1:1 electrolyte at different bulk concentration are compared in Figs. 17 and 18, respectively. The preferential interaction coefficients from the DFT perform a better consistency with the MC than those from the PB equation for both of counterion and co-ion. The better prediction of the DFT is obviously caused by its better estimation of local density of ions than that from the PB.

IV. CONCLUDING REMARKS

A density functional approach has been proposed to calculate the small ion distribution around a model DNA molecule. A WDA approach developed by Yu and Wu [48] is used to evaluate the HS contribution to the free energy functional, while the electrical interaction is obtained through a perturbation around the corresponding uniform fluid. Compared with previous MC and MD results, ionic profiles computed from the present DFT are in good agreement with those from simulations for monovalent or divalent salt in both dilute and concentrated electrolyte solutions.

Electrostatic potential profiles and charge compensation functions predicted by the DFT also agree excellently with computer simulation results. In the mean time, the difference between the PB and MC presenting in ionic profiles is magnified by integration. The relationships among ionic profile, electrostatic potential curve, and charge compensation function are also discussed. It is concluded that the three phenomena, i.e., overshoot of $Q(r)$, change of the sign of $\psi(r)$, and ionic profile overcross, have the same meaning of charge inversion. These three phenomena can be predicted by the DFT, HNC, and computer simulations for multivalent salt at moderate bulk concentration, but never be predicted by the PB equation. Charge inversion is usually overestimated by the HNC at high bulk concentration, but can be predicted correctly by the DFT under the same condition. The higher performance of the DFT is then discussed theoretically and attributes to the superior approximation of the HS correlation. At last, the thermodynamic quantity of preferential interaction coefficient is calculated to characterize the interactions between polyion and one species of small ions. The results from DFT are consistent with the MC results, and better than those from the PB equation.

The model of DNA and small ions considered in this work is somewhat simple and unable to compare with real molecules directly. The models of DNA, which characterize the DNA geometry more accurately, have been applied in computer simulation [54,58]. These models as well as the more elaborated models for small ions may be adopted in our future work. Since the modified fundamental measure theory is applicable to mixtures, the system involving mixed electrolyte solution, similar to that in vivo, can be investigated by some modifications. The work for realistic systems along this line is under study.

ACKNOWLEDGMENT

We gratefully acknowledge the financial support from the National Natural Science Foundation of China (Project Grant No. 20376037).

[1] T. M. Record *et al.*, Annu. Rev. Biochem. **50**, 997 (1981).
[2] G. S. Manning, Q. Rev. Biophys. **11**, 179 (1978).
[3] G. S. Manning, Acc. Chem. Res. **12**, 443 (1979).
[4] C. F. Anderson and T. M. Record, Annu. Rev. Phys. Chem. **33**, 191 (1982).
[5] G. S. Manning, J. Chem. Phys. **51**, 924 (1969).
[6] G. S. Manning, J. Chem. Phys. **51**, 3249 (1969).
[7] G. S. Manning, Biophys. Chem. **7**, 95 (1977).
[8] J. M. Schurr and B. S. Fujimoto, Biophys. Chem. **101–102**, 425 (2002).
[9] J. M. Schurr and B. S. Fujimoto, J. Phys. Chem. B **107**, 4451 (2003).
[10] M. Gouy, J. Phys. (Paris) **9**, 457 (1910).
[11] D. L. Chapman, Philos. Mag. **25**, 475 (1913).
[12] F. Fogolari, P. Zuccato, G. Esposito *et al.*, Biophys. J. **76**, 1 (1999).
[13] M. Fixman, J. Chem. Phys. **70**, 4995 (1979).
[14] J. A. Schellman and H. R. Reese, Biopolymers **16**, 1415 (1977).
[15] S. L. Carnie and G. M. Torrie, Adv. Chem. Phys. **56**, 141 (1984).
[16] L. Degreve and M. Lozada-Cassou, Mol. Phys. **86**, 759 (1995).
[17] W. C. Suh *et al.*, Biochemistry **31**, 7815 (1992).
[18] M. W. Capp, D. S. Cayley, W. Zhang *et al.*, J. Mol. Biol. **258**, 25 (1996).
[19] R. I. Zhdanov, O. V. Rodobed, and V. V. Vlassov, Bioelectrochemistry **58**, 53 (2003).
[20] P. S. Kuhn, Y. Levin, and M. C. Barbosa, Physica A **274**, 8 (1999).
[21] P. L. Felgner and G. M. Ringold, Nature (London) **337**, 387 (1989).
[22] V. A. Bloomfield, Curr. Opin. Struct. Biol. **6**, 334 (1996).
[23] U. P. Strauss, N. L. Gershfeld, and H. Spiera, J. Am. Chem. Soc. **76**, 5909 (1954).
[24] V. I. Perel and B. I. Shklovskii, Physica A **274**, 446 (1999).
[25] A. Y. Grosberg, T. T. Nguyen, and B. I. Shklovskii, Rev. Mod. Phys. **74**, 329 (2002).
[26] E. Trizac, Phys. Rev. E **62**, R1465 (2000).
[27] C. W. Outhwhaite, J. Chem. Soc., Faraday Trans. 2 **74**, 1214 (1978).
[28] C. W. Outhwhaite and L. B. Bhuiyan, Mol. Phys. **74**, 367 (1991).
[29] S. Lamperski and C. W. Outhwhaite, Langmuir **18**, 3423 (2002).
[30] L. B. Bhuiyan and C. W. Outhwhaite, J. Chem. Phys. **116**, 2650 (2002).
[31] T. Das, D. Bratko, L. B. Bhuiyan *et al.*, J. Chem. Phys. **99**, 410 (1995).
[32] T. Das, D. Bratko, L. B. Bhuiyan *et al.*, J. Chem. Phys. **107**, 9197 (1997).
[33] M. Lozada-Cassou, R. Saavedra-Barrera, and D. Henderson, J. Chem. Phys. **77**, 5150 (1982).
[34] G. N. Patey, J. Chem. Phys. **72**, 5763 (1980).
[35] E. Gonzalez-Tovar and M. Lozada-Cassou, J. Chem. Phys. **93**, 3761 (1989).
[36] E. Gonzalez-Tovar, M. Lozada-Cassou, and D. Henderson, J. Chem. Phys. **83**, 361 (1985).
[37] L. Yeomans, S. E. Feller, E. Sanchez *et al.*, J. Chem. Phys. **98**, 1436 (1993).
[38] M. Lozada-Cassou, R. Evans *et al.*, *Fundamentals of Inhomogeneous Fluids* (Marcel-Dekker, New York, 1992).
[39] C. N. Patra and S. K. Ghosh, J. Chem. Phys. **117**, 8938 (2002).
[40] D. Boda, W. R. Fawcett, D. Henderson *et al.*, J. Chem. Phys. **116**, 7170 (2002).
[41] Y.-X. Yu, J. Wu, and G.-H. Gao, J. Chem. Phys. **120**, 7223 (2004).
[42] C. N. Patra and A. Yethiraj, J. Phys. Chem. B **103**, 6080 (1999).
[43] C. N. Patra and A. Yethiraj, Biophys. J. **78**, 699 (2000).
[44] E. Kierlik and M. L. Rosinberg, Phys. Rev. A **44**, 5025 (1991).
[45] M. Deserno *et al.*, J. Phys. Chem. B **105**, 10983 (2001).
[46] L. Mier-y-Teran, E. Diaz-Herrera, M. Lozada-Cassou *et al.*, J. Chem. Phys. **92**, 6408 (1988).
[47] Z. Tang, L. Mier-y-Teran, H. T. Davis *et al.*, Mol. Phys. **71**, 369 (1990).
[48] Y.-X. Yu and J. Wu, J. Chem. Phys. **117**, 10156 (2002).
[49] Y.-X. Yu and J. Wu, J. Chem. Phys. **119**, 2288 (2003).
[50] Y. Rosenfeld, Phys. Rev. Lett. **63**, 980 (1989).
[51] Y. Rosenfeld, J. Chem. Phys. **93**, 4305 (1990).
[52] Y. Rosenfeld, J. Chem. Phys. **98**, 8126 (1993).
[53] V. Vlachy and D. J. Haymet, J. Chem. Phys. **84**, 5874 (1986).
[54] J. C. G. Montoro and J. L. F. Abascal, J. Chem. Phys. **103**, 8273 (1995).
[55] H. Ni, C. F. Anderson, T. M. Record *et al.*, J. Phys. Chem. B **103**, 3489 (1999).
[56] E. Waisman and J. L. Lebowitz, J. Chem. Phys. **56**, 3086 (1972).
[57] E. Waisman and J. L. Lebowitz, J. Chem. Phys. **56**, 3093 (1972).
[58] A. P. Lyubartsev and L. Nordenskiold, J. Chem. Phys. **99**, 10373 (1995).